Journal of Applied Electrochemistry **33**: 497–504, 2003.

Effect of copper additive on $Zr_{0.9}Ti_{0.1}V_{0.2}Mn_{0.6}Cr_{0.05}Co_{0.05}Ni_{1.2}$ alloy anode for nickel–metal hydride batteries

B. HARIPRAKASH, S.K. MARTHA and A.K. SHUKLA*
Solid State and Structural Chemistry Unit, Indian Institute of Science, Bangalore – 560 012, India
*(*author for correspondence, fax: +91 80 3601310, e-mail: shukla@sscu.iisc.ernet.in)*

Received 5 November 2002; accepted in revised form 25 February 2003

Key words: AB_2 alloy, a.c. impedance, nickel–metal hydride batteries

Abstract

$Zr_{1-x}Ti_xV_{0.2}Mn_{0.6}Cr_{0.05}Co_{0.05}Ni_{1.2}$ ($0 \leqslant x \leqslant 0.3$) alloys have been characterized as metal–hydride electrodes for nickel–metal hydride batteries. Although the alloy electrodes with no Ti substitution in place of Zr exhibit a specific capacity value of 375 mA h g^{-1}, it has been possible to enhance the specific capacity of the electrodes to 395 mA h g^{-1} by substituting 10% Ti in place of Zr, that is, with $Zr_{0.9}Ti_{0.1}V_{0.2}Mn_{0.6}Cr_{0.05}Co_{0.05}Ni_{1.2}$ alloy. The specific capacity value of $Zr_{0.9}Ti_{0.1}V_{0.2}Mn_{0.6}Cr_{0.05}Co_{0.05}Ni_{1.2}$ alloy was further enhanced to 415 mA h g^{-1} on copper powder addition. Interestingly, the discharge curves for the latter electrode are quite flat thus providing an advantage of constant specific energy output over the entire regime of electrode discharge. Both a.c. impedance and d.c. linear polarization studies conducted on these electrodes lead to a lower charge-transfer resistance value for the metal-hydride electrode with copper additive suggesting the electrode with copper powder additive to have a higher catalytic activity than those without copper. The electrode with the copper additive also exhibits little change in its capacity over about 100 charge–discharge cycles.

1. Introduction

The rechargeable nickel–metal hydride battery is characteristically akin to the nickel–cadmium battery, which allows ready interchangeability [1]. The principal difference is that the nickel–metal hydride battery uses hydrogen absorbed in an AB_5-type or AB_2-type alloy for the active negative material in place of cadmium used in the nickel–cadmium battery [2]. The AB_2-type alloys are claimed to have a higher capacity for hydrogen to provide superior oxidation and corrosion resistance, and to be less costly [3]. Among the AB_2-type alloys, ZrB_2 (B = Mn, Cr, V) Laves-phase alloys are known to exhibit high specific capacities. However, in order to make these alloys adequate for battery applications, it is mandatory to partially substitute the B-site component with nickel and other appropriate elements [4]. Alternatively, partial substitution of Ti for Zr has also been reported to be equally beneficial [5]. It has also been documented that Zr-based alloy electrodes show remarkable improvement when copper powder is used as an additive [6].

As a part of our ongoing research programme on nickel–metal hydride cells [7–11], in the present study, $ZrV_{0.2}Mn_{0.6}Cr_{0.05}Co_{0.05}Ni_{1.2}$ alloy has been partially substituted with Ti for Zr, and its optimum composition, namely $Zr_{0.9}Ti_{0.1}V_{0.2}Mn_{0.6}Cr_{0.05}Co_{0.05}Ni_{1.2}$, has been studied for the improved effect due to copper addition. It has been possible to achieve a capacity value of *ca.* 415 mA h g^{-1} with such metal-hydride electrodes.

2. Experimental details

Ingots of $Zr_{1-x}Ti_xV_{0.2}Mn_{0.6}Cr_{0.05}Co_{0.05}Ni_{1.2}$ ($0 \leqslant x \leqslant 0.3$) alloy compositions were obtained by arc melting the spongy constituent elements under argon atmosphere at 10^{-3} to 10^{-4} Pa in a water-cooled copper crucible. The powdered alloy ingots were annealed at 1050 °C under argon atmosphere for a week. The alloy samples thus obtained were further powdered and sieved to obtain particles in the range 50–75 μm. Elemental composition of the alloy samples were determined from energy dispersive analysis by X-rays (EDAX) employing a Jeol-JSM-840A scanning electron microscope linked to an Oxford-ISIS elemental analyser by averaging the results from ten randomly chosen spots. Powder X-ray diffraction (XRD) patterns of the alloy samples were obtained on a Siemens-D005 Diffractometer using CuK_α radiation and were indexed using the Proszki algorithm [12].

Roll-compacted electrodes were prepared from the dough obtained by mixing powdered alloy (85 wt %), graphite powder (10 wt %) and polytetrafluroehthylene suspension (5 wt %) in an ultrasonicator. The resultant paste was rolled onto a smooth steel plate and the rolled sheet of the active material with additives was folded

around a degreased nickel mesh (28 mm × 23 mm × 0.02 mm) which was compacted at a pressure of 3000 kg cm^{-2} for 2 min to obtain the metal-hydride electrodes. The roll-compacted electrodes were sintered in a gas stream comprising 10% hydrogen and 90% argon at 350 °C for 30 min. Metal-hydride electrodes with copper additive were prepared similarly but for replacing 70% of graphite with copper powder (Koch Chemicals Ltd, England). The physical thickness of the finished electrodes was about 1 mm. The metal-hydride electrodes thus prepared were subjected to galvanostatic formation in electrochemical cells which contained 6 M KOH as electrolyte and sintered nickel hydroxide electrodes placed on either side of the metal-hydride electrode as counter electrodes.

A.c. impedance in the frequency range between 10 mHz and 10 kHz, and linear d.c. polarization measurements on the electrodes were carried out as a function of their state-of-charge (SOC) values using an Autolab-PGSTAT30 set-up. For both the a.c. impedance and d.c. polarization measurements, the electrodes were fully charged and kept at open-circuit stand for about 2 h for their open-circuit potentials to stabilize. For attaining different SOC values, the electrodes were discharged galvanostatically at $C/5$ rate up to a predetermined period so as to attain the required SOC value. After discharging up to a required SOC value, the cell was kept at open-circuit stand for about 2 h to attain equilibrium. The stable value of open-circuit potential (E_e) was noted and the linear d.c. polarization experiments were carried out within ±15 mV around E_e at a scan rate of 1 mV s^{-1}. The electrodes were left at open-circuit stand for 30 min prior to each impedance measurement. The SOC value of the metal-hydride electrodes was taken as zero at −0.6 V vs Hg/HgO, OH^- (MMO) electrode. The impedance data on the various metal-hydride electrodes were analyzed using a nonlinear least-square fitting program [13]. Temperature-dependent capacity studies on the metal-hydride electrodes were also carried out using specially designed hot and cold chambers. Morphological analyses on the electrodes were carried out on a Jeol-JSM-840A scanning electron microscope both prior and after subjecting them to electrochemical charge–discharge cycling studies.

3. Results and discussion

The chemical composition of various alloy samples employed in the present study is given in Table 1. The powder XRD patterns of various samples given in Figure 1 exhibit well defined peaks corresponding either

Table 1. Compositions of the alloy samples employed during the study

Alloy sample	Alloy compositions aimed at	Alloy compositions as determined by EDAX
1	$ZrV_{0.2}Cr_{0.05}Mn_{0.6}Co_{0.05}Ni_{1.2}$	$Zr_{1.05}V_{0.2}Cr_{0.047}Mn_{0.578}Co_{0.035}Ni_{1.196}$
2	$Zr_{0.9}Ti_{0.1}V_{0.2}Cr_{0.05}Mn_{0.6}Co_{0.05}Ni_{1.2}$	$Zr_{0.9}Ti_{0.11}V_{0.2}Cr_{0.05}Mn_{0.58}Co_{0.042}Ni_{1.2}$
3	$Zr_{0.7}Ti_{0.3}V_{0.2}Cr_{0.05}Mn_{0.6}Co_{0.05}Ni_{1.2}$	$Zr_{0.68}Ti_{0.3}V_{0.2}Cr_{0.02}Mn_{0.6}Co_{0.06}Ni_{1.24}$

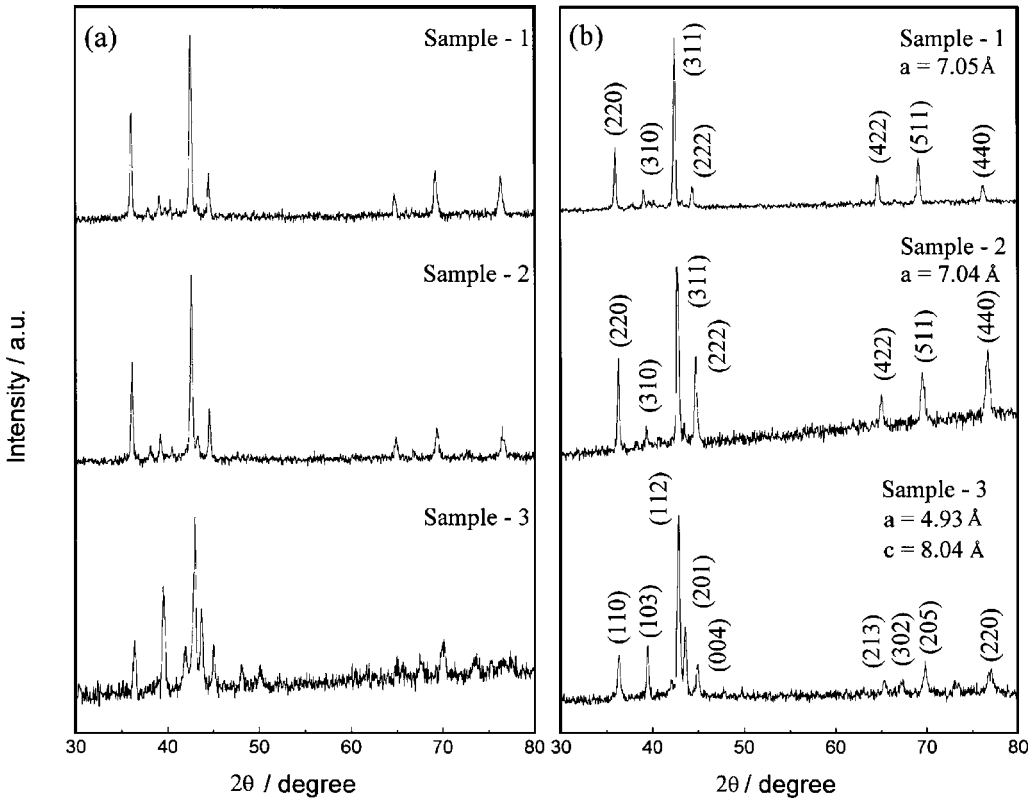

Fig. 1. Powder XRD patterns of the alloy samples (a) as prepared, and (b) after annealing.

to the cubic C15 or hexagonal C14 Laves phase structures. Mixed phases of Zr_7Ni_{10} and Zr_9Ni_{11} are seen in as prepared alloy samples (Figure 1(a)) while the presence of Zr_7Ni_{10} phase is observed in annealed samples (Figure 1(b)) [4].

The electrode formation data for electrodes obtained from various alloy samples are presented in Figure 2. While the metal-hydride electrodes without any copper powder additive form and achieve their stable capacity values within 10–15 charge–discharge cycles those with copper powder additive form within 6–7 charge–discharge cycles as shown in Figure 2. Several approaches have been adopted to increase the activation behavior of metal-hydride electrodes [14–21]. It is evident that metal-hydride electrodes comprising $Zr_{0.9}Ti_{0.1}V_{0.2}Mn_{0.6}Cr_{0.05}Co_{0.05}Ni_{1.2}$ and copper additive deliver the highest capacity. A typical charge–discharge data for such an electrode is presented in Figure 3. The galvanostatic discharge capacity data obtained at a discharge current density of 80 mA g^{-1} for various alloy electrodes is given in Figure 4. Among all the electrodes, the discharge curve for the electrode with copper powder additive is quite flat hence providing an advantage of constant specific energy out-put over the entire regime of the electrode discharge. The flat discharge curve is also indicative of a discharge where the effect of change in reactants and reaction products is minimal until the active materials are nearly exhausted.

To further examine the effect of copper powder additive on the performance of alloy electrodes, we have carried out impedance study as a function of state-of-charge values of the electrodes and the data are shown in Figure 5. It has been possible to fit the impedance plots for the various alloy electrodes at all SOC values to a R_Ω (R_1Q_1) (R_2Q_2) equivalent circuit, shown in an inset to Figs. 5(a)–5(d), using a non-linear least-square fitting program [22, 23]. The impedance spectrum comprising two semicircles is due to two pairs of parallel resistances and capacitances. However, the semicircles are depressed with their centers below the real axis. Accordingly, a constant phase element (CPE) is considered in place of a capacitance. Consequently, R_1 and Q_1 are the respective values for resistance and CPE corresponding to the high-frequency semicircle, and R_2 and Q_2 are the respective values for resistance and CPE corresponding to the low-frequency semicircle. It is noteworthy that while R_1 is the resistance due to morphology of the porous-electrode subsequent to its formation, R_2 refers to the charge-transfer resistance for the electrode reaction. The two constant phase elements Q_1 and Q_2 refer to the capacitance due to the porous-electrode morphology and electrode double-layer capacitance, respectively.

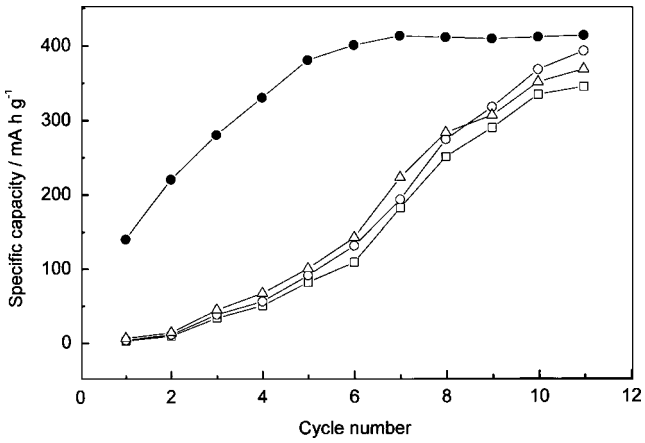

Fig. 2. Discharge capacity data obtained at 25 °C during formation cycles for metal-hydride electrodes comprising (□) sample 1, (○) sample 2, (△) sample 3 and (●) sample 2 + Cu.

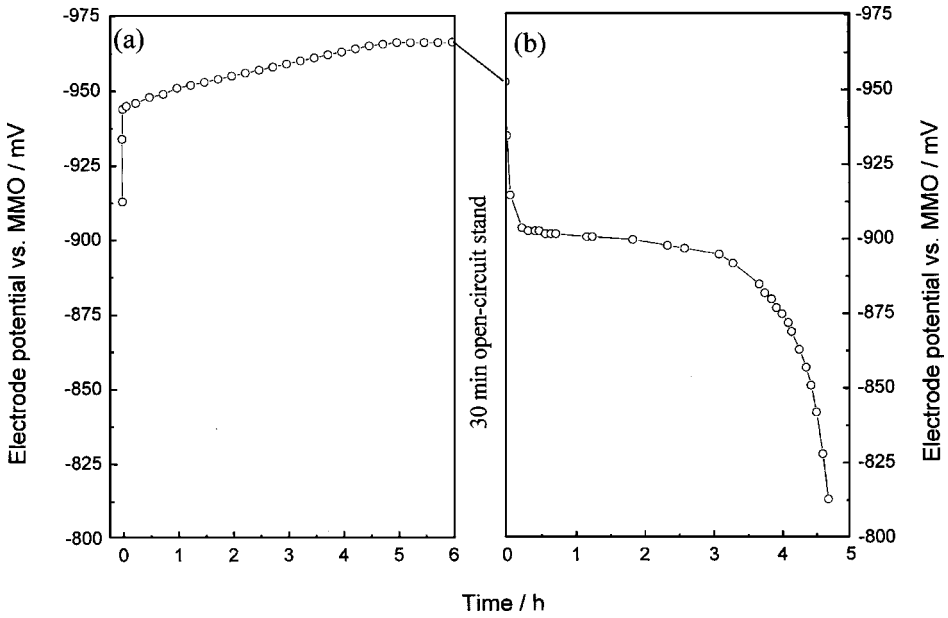

Fig. 3. Typical charge–discharge data at $C/5$ rate for a metal-hydride electrode of sample 2 having copper additive obtained at 25 °C.

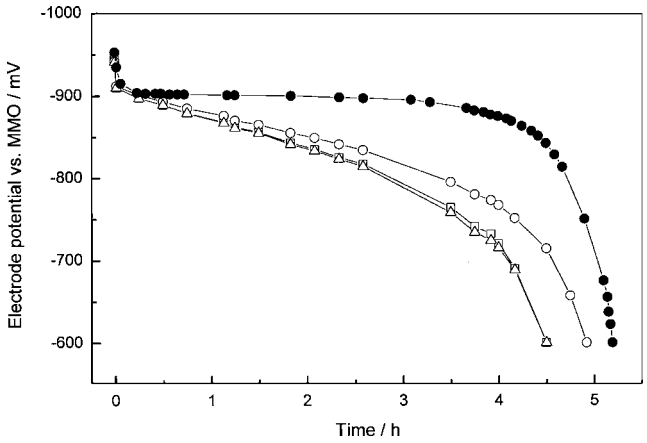

Fig. 4. Discharge curves obtained at a load current density of 80 mA g^{-1} for metal-hydride electrodes comprising (□) sample 1, (○) sample 2, (△) sample 3 and (●) sample 2 + Cu, at 25 °C.

From the impedance data, it is evident that the electrode reaction is primarily activation controlled. In the above scheme for fitting the impedance data, R_Ω refers to the ohmic resistance comprising electrolyte resistance, resistance due to electrode material and the resistance due to the electrical contacts. It is noteworthy that while the R_1 value ranges between 22 and 97 mΩ for SOC values between 1 and 0 for electrodes without copper additive, the R_1 value for the alloy sample 2 electrode with copper additive ranges between 26 and 36 mΩ for SOC values between 1 and 0. This clearly shows that the morphology of the alloy sample 2 electrodes with copper additive is different from those without copper additive. The charge-transfer resistance (R_{ct}) values for various alloy electrodes as obtained from the impedance plots at different SOC values are shown in Figure 6. The data show that the alloy having 10% of titanium in A-site, namely $Zr_{0.9}Ti_{0.1}V_{0.2}Mn_{0.6}Cr_{0.05}Co_{0.05}Ni_{1.2}$ exhibits the least R_{ct} value and hence is most adequate for battery applications. Ohmic resistance values for all the metal-hydride electrodes reported here happen to be less than 50 mΩ.

We also carried out discharge experiments for electrodes with and without copper additive at $C/5$, $C/3$, C, $2C$ and $3C$ rates at 25 °C, and data are shown in Figure 7. These data show that metal-hydride electrodes with copper additive have distinct advantage in relation to those without copper additive at all discharge rates. Similar findings have been reported [5, 24]. Metal-hydride electrodes with copper additive deliver a discharge capacity of 53% at $3C$ rate in relation to the electrode capacity value at the $C/5$ rate. By contrast, metal-hydride electrodes without any copper powder additive delivered a capacity of 46% at $3C$ rate in relation to the electrode capacity value at the $C/5$ rate. We also conducted linear-polarization experiments on metal-hydride electrodes at different SOC values for electrodes with and without copper additive. Linear-polarization data at various SOC values for the metal-

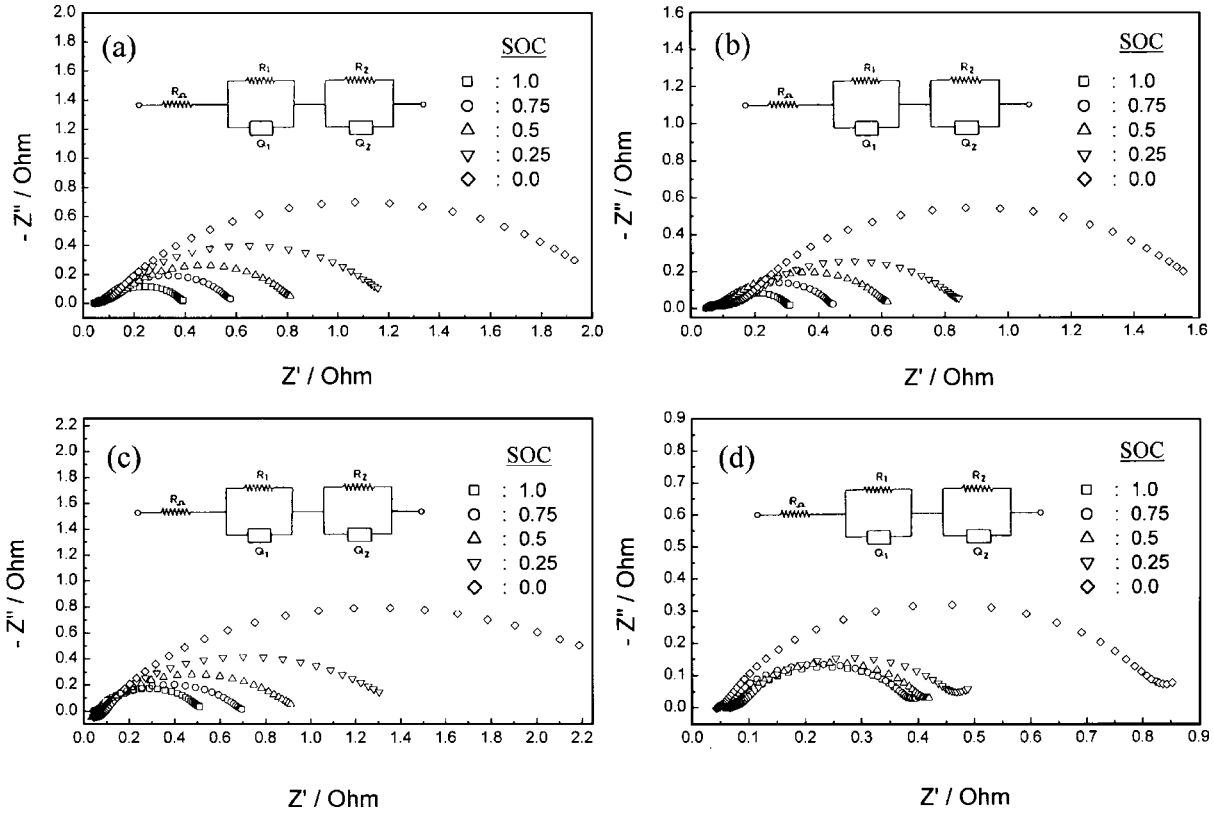

Fig. 5. Electrochemical impedance spectra obtained at 25 °C for metal-hydride electrodes comprising (a) sample 1, (b) sample 2, (c) sample 3, and (d) sample 2 + Cu. Equivalent circuit employed to fit the impedance data is also shown in the inset.

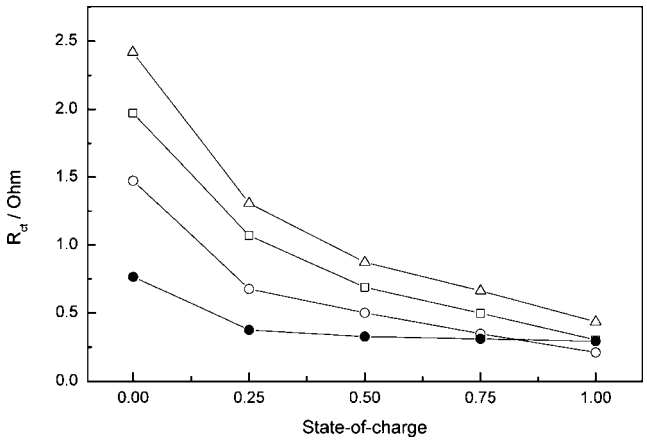

Fig. 6. Charge-transfer resistance values as a function of state-of-charge for metal-hydride electrodes comprising (□) sample 1, (○) sample 2, (△) sample 3 and (●) sample 2 + Cu.

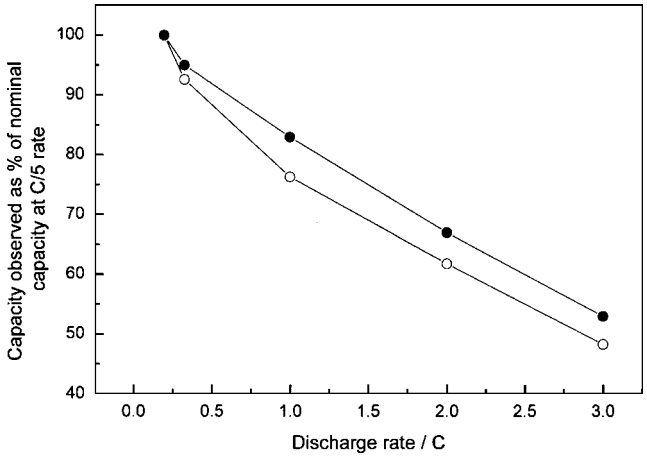

Fig. 7. High-rate discharge data obtained at 25 °C for the electrodes of sample 2 (○) without copper additive, and (●) with copper additive.

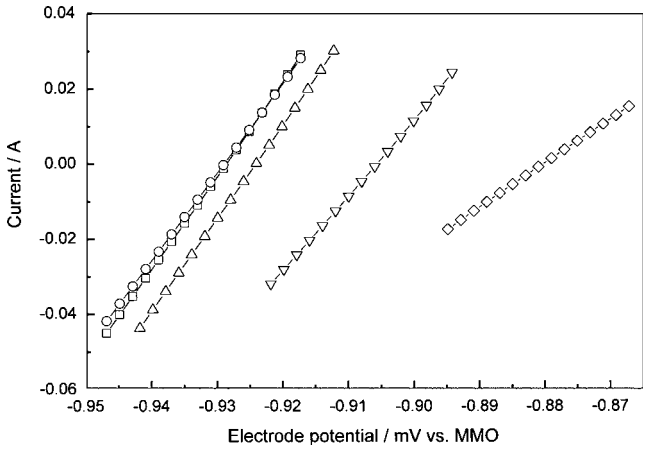

Fig. 8. Linear-polarization data obtained at 25 °C as a function of state-of-charge for the electrode of alloy sample 2 with copper additive. SOC: (□) 1.0, (○) 0.75, (△) 0.5, (▽) 0.25 and (◇) 0.0.

hydride electrode having copper additive are shown in Figure 8. R_{ct} values for metal-hydride electrodes were also calculated from the linear-polarization measurements and were found to be in good agreement with those obtained from impedance measurements. The R_{ct} values for metal-hydride electrodes derived from impedance measurements were used for calculation of exchange current density values at different SOC values. The exchange current density values obtained for all the metal-hydride electrodes studied here at various SOC values are given in Table 2. Data show a higher exchange current density value at all SOC values for metal-hydride electrodes with copper additive. This shows that the activity of metal-hydride electrode is enhanced by addition of copper. These exchange current density values are higher than the values reported for both the La-based AB_5 alloys [25, 26] and Zr-based AB_2 alloys [27, 28], but are lower than cerium-substituted La-based AB_5 alloys [29].

The faradaic efficiency of the metal-hydride electrodes at 25 °C at the $C/5$ rate is about 98% for the 100% charge input. Metal-hydride electrodes with copper additive were also subjected to a charge stand for 12 days and were found to retain about 95% of their nominal capacity. This suggests that the self-discharge rate of these electrodes is about 0.4% per day which is well within the self-discharge rates for alloy electrodes reported in the literature [1, 30, 31]. Temperature-dependent capacity measurements on the electrodes were also conducted and data considering the discharge capacity at 25 °C at $C/5$ rate to be 100% are shown in Figure 9. Metal-hydride electrodes with copper additive delivered more than 50% of capacity at −40 °C. At higher temperatures, these electrodes delivered lesser capacity in relation to the electrode capacity at 25 °C [32]. Peukert plots for alloy sample electrodes with and without copper additive are shown in Figure 10. From these Peukert plots, we obtained values of n in the Peukert relationship, $I^n t = a$, where I is the discharge current, t is the discharge time and n and a are constants [33]. The values of n for alloy electrodes with and without copper additive are 0.83 and 0.74, respectively, which suggest a higher faradaic efficiency for the electrode with copper additive.

Metal-hydride electrodes were also subjected to charge–discharge cycle-life test at $C/5$ rate and data shown in Figure 11 depict little loss in the nominal capacity of the electrodes up to 100 cycles. In literature [34–36], several approaches have been attempted to suppress the capacity loss during electrode cycling. It has been reported that the charge–discharge characteristics of metal-hydride electrodes can be improved to a greater extent by microencapsulation of the alloy powder with a thin copper layer [37]. We also believe that the copper addition protects the alloy surface from oxidation facilitating the charge-transfer reaction on the alloy surface. This also decreases irreversible losses in electrode capacities [6, 31].

A knowledge of change in morphology of the metal-hydride particles during electrode charge–discharge processes is important to reflect on the performance characteristics of the electrodes [38]. Therefore, scanning

Table 2. Exchange current density values obtained for various alloy electrodes as a function of their SOC values

SOC Value	Exchange current density							
	Sample 1 /mA cm^{-2}	/mA g^{-1}	Sample 2 /mA cm^{-2}	/mA g^{-1}	Sample 3 /mA cm^{-2}	/mA g^{-1}	Sample 2 + Cu /mA cm^{-2}	/mA g^{-1}
1.00	30.0	241.8	43.0	346.1	21.0	168.8	31.1	250.0
0.75	18.4	147.8	26.2	210.6	14.2	114.5	29.4	236.4
0.50	13.3	107.0	18.2	146.9	10.5	84.4	27.9	224.8
0.25	8.6	68.9	13.5	108.9	7.0	56.4	24.4	196.1
0.00	4.6	37.4	6.2	50.0	3.8	30.5	12.0	96.3

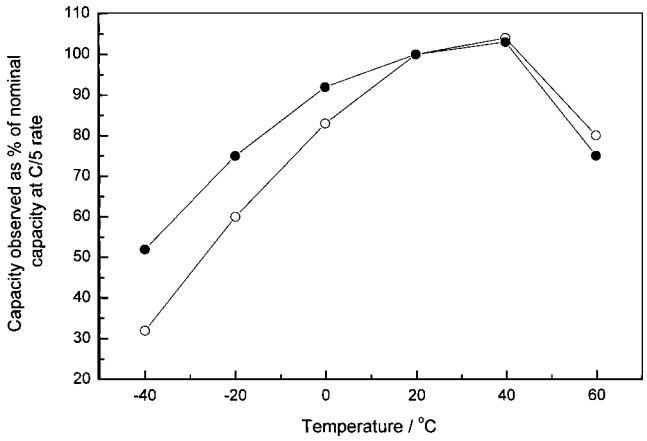

Fig. 9. Low-temperature dischargeability of the electrodes of sample 2 (○) without copper additive and (●) with copper additive.

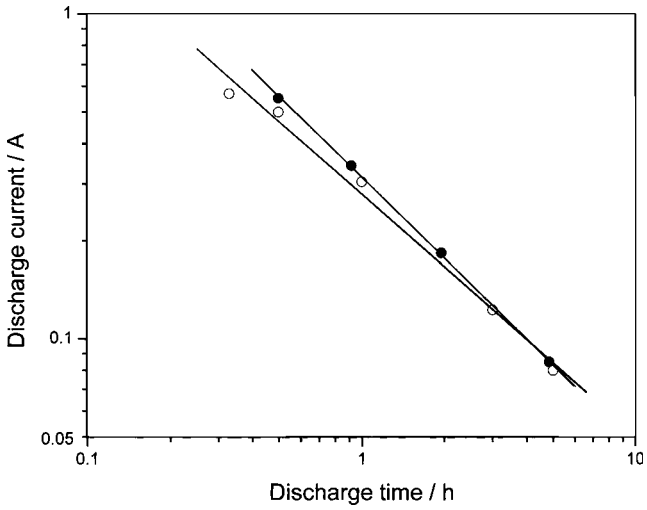

Fig. 10. Peukert plots at 25 °C for the electrodes of sample 2 (○) without copper additive, and (●) with copper additive.

electron micrographs for various alloy electrodes were also obtained prior and after their cycle-life tests as shown in Figures 12 and 13. As seen from the electron micrographs, the alloy particles were free from any surface cracks prior to charge–discharge cycling of the electrodes. However, subsequent to cycling, morphology of the alloy electrodes changed significantly and microcracks were found to develop in the bulk alloys owing to its volumetric deformation due to absorption/desorption of hydrogen. Interestingly, the micrographs for metal-hydride electrodes with copper additive show distinct morphological changes after charge–discharge cycling in relation to other electrodes which is in conformity with the impedance data.

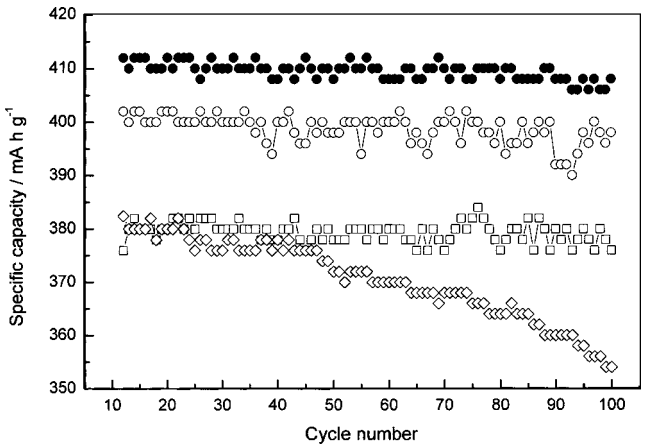

Fig. 11. Cycle-life data obtained at 25 °C for metal-hydride electrodes comprising (□) sample 1, (○) sample 2, (◇) sample 3 and (●) sample 2 + Cu at $C/5$ rate.

4. Conclusions

$Zr_{1-x}Ti_xV_{0.2}Mn_{0.6}Cr_{0.05}Co_{0.05}Ni_{1.2}$ $(0 \leqslant x \leqslant 0.3)$ alloy electrodes have been characterized electrochemically and the effect of copper powder additive on $Zr_{0.9}Ti_{0.1}V_{0.2}Mn_{0.6}Cr_{0.05}Co_{0.05}Ni_{1.2}$ alloy electrodes, which exhibit the highest discharge capacity, has been investigated. It has been found that the performance of the $Zr_{0.9}Ti_{0.1}V_{0.2}Mn_{0.6}Cr_{0.05}Co_{0.05}Ni_{1.2}$ alloy electrode improves on inclusion of the copper powder additive and the exchange current densities for this electrode are higher in relation to other electrodes at all SOC values. This electrode exhibits a discharge capacity of 83% at C rate in relation to its maximum value at $C/5$ rate. At −40 °C, this electrode exhibits a discharge capacity of 52% in relation to its maximum value at 27 °C at $C/5$ rate. The electrode with copper additive exhibited little change in its discharge capacity value of 415 mA h g^{-1} over 100 charge–discharge cycles conducted during the study.

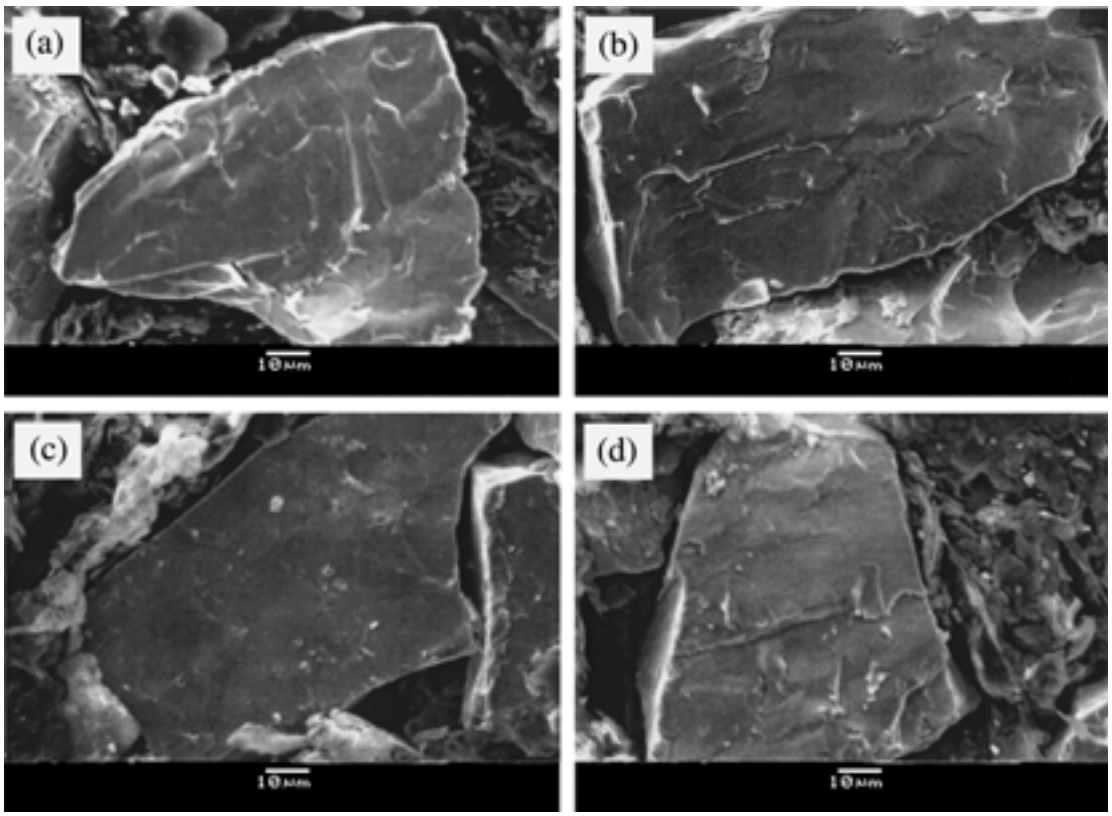

Fig. 12. Scanning electron micrographs for the electrodes comprising (a) sample 1, (b) sample 2, (c) sample 3, and (d) sample 2 + Cu prior to their cycling.

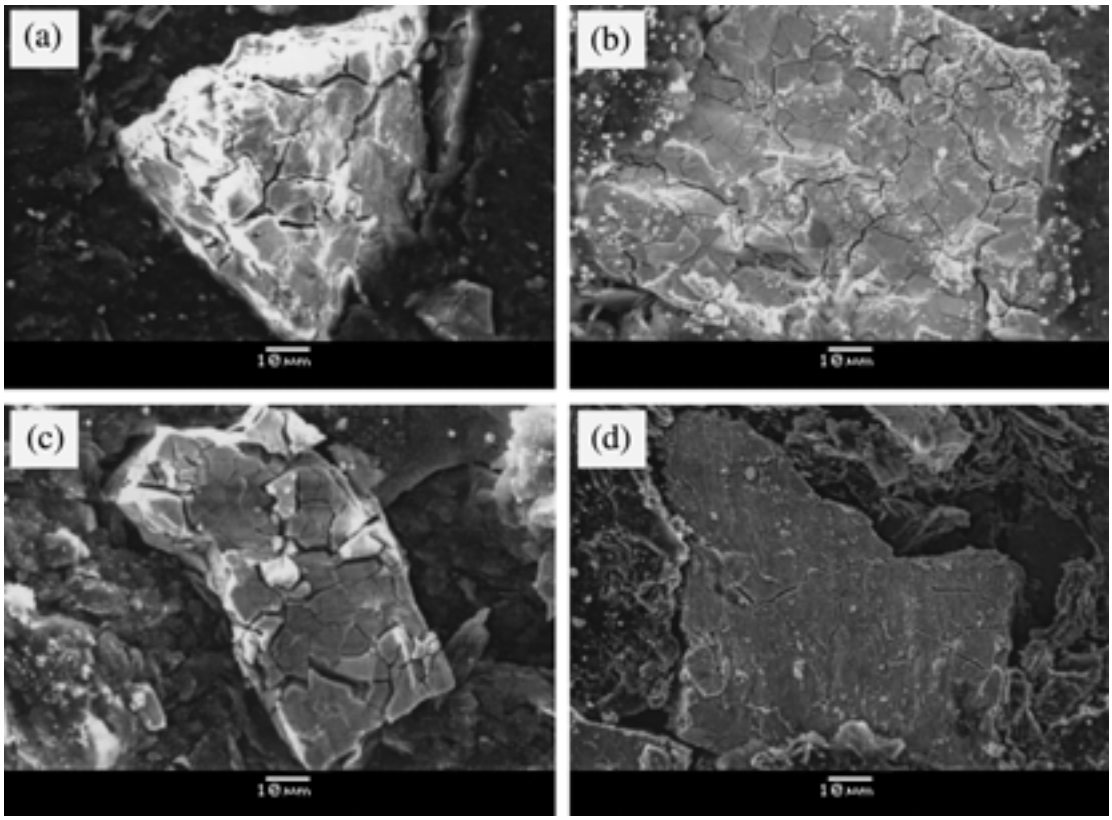

Fig. 13. Scanning electron micrographs for the electrodes comprising (a) sample 1, (b) sample 2, (c) sample 3 and (d) sample 2 + Cu subsequent to their cycling.

Acknowledgements

We thank Dr V. Ganesh Kumar and Dr K. M. Shaju for their invaluable help during this study.

References

1. C.A. Vincent and B. Scrosati, 'Modern Batteries', (Arnold, London, 1997).
2. A.K. Shukla, S. Venugopalan and B. Hariprakash, *J. Power Sources* **100** (2001) 125.
3. R.M. Dell and D.A.J. Rand, 'Understanding Batteries'. (Royal Society of Chemistry, Cambridge, UK 2002).
4. B. Knosp, C. Jordy, Ph. Blanchard and T. Berlureau, *J. Electrochem. Soc.* **145** (1998) 1478.
5. D-M. Kim, S-W. Jeon and J-Y. Lee, *J. Alloys Comp.* **279** (1998) 209.
6. J.S. Yu, H. Lee, P.S. Lee and J.Y. Lee, *J. Electrochem. Soc.* **147** (2000) 2494.
7. V. Ganesh Kumar, N. Munichandriah and A.K. Shukla, *J. Power Sources* **63** (1996) 203.
8. V. Ganesh Kumar, K.M. Shaju, N. Munichandraiah and A.K. Shukla, *J. Power Sources* **76** (1998) 106.
9. S. Rodrigues, N. Munichandriah and A.K. Shukla, *J. Appl. Electrochem.* **29** (1999) 1285.
10. K.M. Shaju, V. Ganesh Kumar, S. Rodrigues, N. Munichandriah and A.K. Shukla, *J. Appl. Electrochem.* **30** (2000) 347.
11. S. Rodrigues, N. Munichandriah and A.K. Shukla, *Proc. Indian Acad. Sci.* **113**, (2001) 527.
12. W. Losocha and K. Lewinski, *J. Appl. Crystallogr.* **27** (1994) 437.
13. B.A. Boukamp, '*Equivalent Circuit*', Users Manual (University of Twente, The Netherlands, 1989).
14. J-S. Yu, H. Lee, S-M. Lee and J-Y. Lee, *J. Electrochem. Soc.* **146** (1999) 4366.
15. H. Lee, S-M. Lee and J-Y. Lee, *J. Electrochem. Soc.* **146** (1999) 3666.
16. W.K. Choi, S.G. Zhang, J.I. Murayama, R.S. Ya, H. Inoue and C. Iwakura, *J. Alloys Comp.* **280** (1998) 99.
17. M.S. Wu, H.R. Wu, Y.Y. Wang and C.C. Wan, *J. Alloys Comp.* **302** (2000) 248.
18. A. Zuttel, F. Meli and L. Schlapbach, *J. Alloys Comp.* **209** (1994) 99.
19. J-H. Jung, H-H. Lee, D-M. Kim, B-H. Liu, K-Y. Lee and J-Y. Lee. *J. Alloys Comp.* **253–254** (1997) 652.
20. S-M. Lee, D-M. Kim, J-S. Yu, K-J. Jang and J-Y. Lee, *J. Electrochem. Soc.* **145** (1998) 1953.
21. X.L. Wang and S. Suda, *J. Alloys Comp.* **231** (1995) 380.
22. N. Kuriyama, T. Sakai, H. Miyamura I. Uehara, H. Ishikawa and T. Iwasaki, *J. Alloys Comp.* **202** (1993) 183.
23. W. Zhang, M.P. Sridhar Kumar and S. Srinivasan, *J. Electrochem. Soc.* **142** (1995) 2935.
24. M. Geng, J. Han, F. Feng and D.O. Northwood, *J. Electrochem. Soc.* **146** (1999) 3591.
25. G. Zheng, B.N. Popov and R.E. White, *J. Electrochem. Soc.* **143** (1996) 834.
26. B.N. Popov, G. Zheng and R.E. White, *J. Appl. Electrochem.* **26** (1996) 603.
27. J. Chen, D-H. Bradhurst, S-X. Dou and H-K. Liu, *J. Alloys Comp.* **265** (1998) 281.
28. D-M. Kim, S-M. Lee, K-J. Jang and J-Y. Lee, *J. Alloys Comp.* **268** (1998) 241.
29. H. Ye, B. Xia, W. Wu, K. Du and H. Zhang, *J. Power Sources* **111** (2002) 145.
30. S.R. Ovshinsky, M.A. Fetcenko and J. Ross, *Science* **260** (1993) 176.
31. C. Iwakura, Y. Kajiya, H. Yoneyama, T. Sakai, K. Oguro and H. Ishikawa, *J. Electrochem. Soc.* **136** (1989) 1351.
32. C. Jeong, W. Chung, C. Iwakura and I. Kim, *J. Power Sources* **79** (1999) 19.
33. D. Linden and T.B. Reddy, '*Handbook of Batteries*', (McGraw-Hill, New York, 2002).
34. J-S. Yu, S-M. Lee, K. Cho and J-Y. Lee, *J. Electrochem. Soc.* **147** (2000) 2013.
35. H. Miyamura, T. Sakai, N. Kuriyama, K. Oguro, I. Uehara and H. Ishikawa, *Z. Phy. Chem.* **183** (1994) 347.
36. M.A. Fetcenko, S. Venkatesan and S.R. Ovshinsky, *in* D.A. Corrigan and S. Srinivasan (Eds), '*Hydrogen storage materials, Batteries, and Electrochemistry*', (The Electrochemical Society Proceedings Series, Pennington, NJ, 1992), p. 41.
37. T. Sakai, H. Ishikawa, K. Oguro, C. Iwakura and H. Yoneyama, *J. Electrochem. Soc.* **134** (1987) 558.
38. W. Zhang, A. Visintin, S. Srinivasan, A.J. Appleby and H.S. Lim, *J. Power Sources* **75** (1998) 84.